ENSO contribution to the assessment of long-term cloud feedback on global warming

Huan Liu[1], Ilan Koren[2], Orit Altaratz[2], Shutian Mu[1]

[1]College of Meteorology and Oceanography, National University of Defense Technology, Changsha, 410073, China
[2]Department of Earth and Planetary Sciences, Weizmann Institute of Science, Rehovot, 76100, Israel

Correspondence to: Huan Liu (huanliu@nudt.edu.cn)

Abstract. Accurately assessing cloud feedback on global warming is essential for producing reliable climate projections. Linear regression analysis is a widely used method for this purpose, offering a straightforward approach for examining the relationship between cloud radiative effects and global-mean surface temperature. However, the El Niño–Southern Oscillation (ENSO) can significantly contribute to these estimates, which is often overlooked due to ENSO's relatively short periodicity (2–7 years). Using 72 years of reanalysis data and 150 years of simulations by 11 global climate models, this study demonstrates that, over a large portion of the low- to mid-latitude oceans, ENSO can contribute up to a few W m^{-2} K^{-1} to the regression-based cloud feedback estimates over decades and even centuries. Through a detailed spatial and temporal analysis, our findings underscore the importance of accounting for and removing ENSO's influence to improve the accuracy of cloud feedback assessments in the context of global warming.

1 Introduction

Clouds, which cover over 50% of the Earth's surface, play a critical role in regulating the Earth's energy budget (Stubenrauch et al., 2013). They reflect incoming solar radiation (shortwave cloud radiative effect, CRE_{SW}) and trap outgoing terrestrial radiation (longwave cloud radiative effect, CRE_{LW}), resulting in a net cooling effect (net cloud radiative effect, CRE_{net}) of approximately 20 W m^{-2} at the top of the atmosphere (TOA) (Stephens et al., 2012). This fundamental role makes cloud response to global warming (cloud feedback) a key factor in climate change projections (Zelinka et al., 2020). While Sherwood et al. (2020) constrained the cloud feedback to be positive (amplifying warming), its magnitude remains highly uncertain across current global climate models (GCMs). This uncertainty is the dominant source of the spread in equilibrium climate sensitivity estimates (Forster et al., 2021).

One major source of the uncertainty in estimates of cloud feedback on global warming is natural climate variability, caused by phenomena such as the Atlantic Multi-decadal Variability, the Pacific Decadal Oscillation, and the El Niño-Southern Oscillation (ENSO) (Li et al., 2021), all of which can introduce distinct spatial and temporal influences across different regions and periods (Forster et al., 2021). ENSO is characterized by anomalous sea-surface temperatures and sea-level pressure in the tropical Pacific, operating on relatively short timescales with a typical periodicity of 2–7 years (Neelin et al., 1998). By

modulating atmospheric dynamics and thermodynamics (Davey et al., 2014; Taschetto et al., 2020), ENSO affects cloud properties (Park and Leovy, 2004; Eleftheratos et al., 2011; Teng et al., 2014; Madenach et al., 2019; Liu et al., 2023) and CREs (Chen et al., 2000; Yang et al., 2016). Previous studies have identified an ENSO signature, on a global scale, in both the long-term warming trend (e.g., Penland and Matrosova, 2006; Compo and Sardeshmukh, 2010) and cloud feedback estimates (hereafter referred to as the ENSO contribution) (e.g., Zhou et al., 2015; Richardson et al., 2022; Uribe et al., 2022; Jin et al., 2024). For example, Richardson et al. (2022) proposed that ENSO contribution may affect estimated linear trends over short time windows of up to about 10 years. Jin et al. (2024) found that the seasonally asymmetric patterns of cloud feedback are primarily controlled by ENSO. Nevertheless, the full influence of ENSO on cloud feedback in the context of global warming remains unclear and has often been overlooked due to ENSO's relatively short periodicity (Hope et al., 2017).

To partially address this knowledge gap, we apply a regression-based method to correct for ENSO's influence (hereafter referred to as the ENSO-correction method), thereby quantifying the spatial distribution and timescales of ENSO contribution to cloud feedback estimates under global warming. The remainder of this paper is organized as follows: Section 2 describes the datasets and methodology, Section 3 presents the key findings, and Section 4 summarizes the main conclusions.

2 Materials and methods

2.1 Datasets

The primary analysis uses 72 years of reanalysis data from the ERA5 dataset, 20 years of satellite measurements from the CERES EBAF product, and 150 years of GCM simulations from the abrupt-4×CO_2 experiment. For supplementary analysis, a 65-year segment of GCM simulations from the historical experiment is also used. The analysed variables include sea-surface temperature, air temperature at 2 meters, all-sky and clear-sky TOA shortwave fluxes, as well as all-sky and clear-sky TOA longwave fluxes. The details of the different datasets are as follows:

(1) ERA5 data (January 1950–December 2021). Monthly ERA5 data (Hersbach et al., 2023) are used to analyze the ENSO contribution to historical cloud feedback estimates. To illustrate the method and results (a sample analysis), a representative 40-year subset (January 1982–December 2021) is used. ERA5 is a well-validated and widely used dataset for studying climate trends, produced by the European Centre for Medium-Range Weather Forecasts (ECMWF) (Hersbach et al., 2020; Gulev et al., 2021). ERA5 data show strong agreement with observed cloud properties across both weather and climate scales and have been found to effectively capture the spatiotemporal characteristics of measured ENSO-driven changes in cloud cover (Liu et al., 2023; Yao et al., 2020; Binder et al., 2020).

(2) CERES measurements (January 2002–December 2021). We compare the ENSO contribution derived from ERA5 data with that from satellite measurements using TOA fluxes from the Clouds and the Earth's Radiant Energy System (CERES) Energy Balanced and Filled (EBAF) data product (Loeb et al., 2018; updated to Edition 4.2). The product is specifically designed for climate trend analysis, as it minimizes errors from instrument calibration and orbital drift by integrating

measurements from multiple satellites (Loeb et al., 2018). Here, this product is regarded as a benchmark observational dataset for evaluating reanalysis estimates of the Earth's energy budget.

(3) GCM simulations (January 1950–December 2014 for the historical experiment, and the first 150 years for the abrupt-4×CO_2 experiment). This study uses simulations from the historical and abrupt-4×CO_2 experiments conducted by 11 GCMs participating in the Cloud Feedback Model Intercomparison Project (CFMIP) of the sixth phase of the Coupled Model Intercomparison Project (CMIP6) (Webb et al., 2017). We focus on the simulation variant "r1i1p1f1" (Eyring et al., 2016). The historical experiment spans from 1850 to 2014 and is designed to provide insights into how the observed natural and anthropogenic factors have shaped current climate conditions. In this study, the period of January 1950–December 2014 is analyzed to generalize the results obtained from ERA5 data. The abrupt-4×CO_2 experiment is a Diagnostic, Evaluation and Characterization of Klima (DECK) experiment with a mandated minimum simulation period of 150 years. It is designed to evaluate the climate response to an instantaneous quadrupling of the prescribed pre-industrial atmospheric CO_2 concentration and is therefore widely used for assessing cloud feedback in the context of global warming. We use the first 150 years of these simulations to investigate the ENSO contribution to cloud feedback projections.

Table 1: Information of GCM simulations used in this study.

GCM	Center	Country	Data Version		Data DOI
			Historical	Abrupt-4×CO_2	
E3SM-1-0	UCSB, E3SM-Project, UCI	USA	v20190913	v20190718	10.22033/ESGF/CMIP6.2294
CESM2	NCAR	USA	v20190308	v20190927	10.22033/ESGF/CMIP6.2185
BCC-CSM2-MR	BCC	China	v20181126	v20181016	10.22033/ESGF/CMIP6.1725
CanESM5	CCCma	Canada	v20190429	v20190429	10.22033/ESGF/CMIP6.1303
MRI-ESM2-0	MRI	Japan	v20190222	v20190308	10.22033/ESGF/CMIP6.621
IPSL-CM6A-LR	IPSL	France	v20180803	v20190118	10.22033/ESGF/CMIP6.1534
GFDL-CM4	NOAA-GFDL	USA	v20180701	v20180701	10.22033/ESGF/CMIP6.1402
GISS-E2-1-H	NASA-GISS	USA	v20190403	v20190403	10.22033/ESGF/CMIP6.1421
GISS-E2-2-G	NASA-GISS	USA	v20191120	v20191120	10.22033/ESGF/CMIP6.2081
MIROC6	MIROC	Japan	v20181212	v20190705	10.22033/ESGF/CMIP6.881
NorESM2-LM	NCC	Norway	v20190815	v20210118	10.22033/ESGF/CMIP6.502

2.2 Data processing

All datasets are resampled and regridded to a common spatial resolution of 2°×2° to reduce computational demands. We first derive the oceanic Niño index (ONI) from these data to quantify ENSO activity. The ONI is calculated as the area-weighted 3-month running mean of sea-surface temperature anomalies (units: K) over the Niño 3.4 region (5° S–5° N, 170° W–120° W). For each dataset, anomalies are defined relative to the climatology over the corresponding study period (see Section 2.1). ONI is the primary indicator used by the National Oceanic and Atmospheric Administration (NOAA) for monitoring the oceanic component of ENSO and is widely used in related studies (Glantz and Ramirez, 2020). Periods with large positive or negative ONI values indicate intense warm or cold phases of ENSO (i.e., the El Niño or La Niña events), which are

characterized by unusual warming or cooling of the central and eastern tropical Pacific Ocean surface waters, respectively (Neelin et al., 1998). Then, for each dataset, we apply the following two-step approach:

(1) Calculation of monthly means. Monthly mean CREs are derived as follows: CRE_{SW} and CRE_{LW} are calculated as the differences between all-sky and clear-sky TOA shortwave and longwave fluxes, respectively; CRE_{net} is obtained by summing CRE_{SW} and CRE_{LW}. The monthly global mean surface temperature (GMST) is calculated as the area-weighted mean of air temperature at 2 meters.

(2) Calculation of monthly anomalies. Monthly anomalies of CRE_{SW}, CRE_{LW}, CRE_{net}, and GMST are calculated as deviations of each variable from its mean annual cycle and hence are deseasonalized. This is done by subtracting, for each calendar month, the long-term mean (calculated over the entire study period) from the corresponding monthly value.

The area-weighted means are calculated based on grid cell area to correct for the over-representation of high-latitude regions where grid cells smaller. The area of each grid cell is estimated as the product of arc length at the corresponding latitude and longitude, considering the Earth as an oblate spheroid with a radius of 6,378.137 km at the equator and 6,356.752 km at the poles. The statistical significance of temporal trends (trends over time) and partial regression coefficients is assessed using the Hamed and Rao modified Mann-Kendall trend test (Hamed and Rao, 1998; Hussain and Mahmud, 2019) and Student's t-test, respectively. The modified Mann-Kendall test is a non-parametric method that effectively accounts for serial autocorrelation.

2.3 The ENSO-correction method

The ENSO-correction method is applied to isolate and remove the ENSO signal from the CRE and GMST records. Various approaches have been developed for this purpose, including those based on numerical simulations and statistical techniques such as frequency bandpass filtering, regression, and signal decomposition (Penland and Matrosova, 2006; Compo and Sardeshmukh, 2010; Kelly and Jones, 1996; Angell, 2000; Guan and Nigam, 2008).

In this study, we employ a regression-based ENSO-correction method due to its conceptual simplicity and computational efficiency. Specifically, because the ONI is calculated without explicitly removing the long-term warming trend, we first use a bandpass filter to retain only the variability within the typical ENSO periodicity band of 2–7 years (Fig. 1). This filtering effectively eliminates linear trends and decouples the core ENSO signal from other climate perturbations, such as the Atlantic Multi-decadal Variability and the Pacific Decadal Oscillation. Then we use an ordinary least squares (OLS) regression to establish astatistical relationship between a dependent variable (Y; e.g., CRE_{SW}, CRE_{LW}, CRE_{net} or GMST) and the independent variables of time and the bandpass-filtered ONI, assuming no time lag. This yields a multivariate regression model formulated as Eq. (1):

$$\hat{Y} = a \times time + b \times ONI_{filtered} + c \quad (1),$$

which minimizes the sum of squared residuals (Virtanen et al., 2020). Therefore, the residual derived from this model (referred to as the ENSO-corrected series), as formulated by Eq. (2):

$$\hat{Y}_{ENSO-corrected} = Y - b \times ONI_{filtered} \quad (2),$$

removes the linear ENSO signature while effectively preserving the underlying temporal trend in Y. Importantly, because Eq. (1) uses the bandpass-filtered ONI and assumes no time lag, this OLS-based ENSO-correction method may retain some ENSO-related variations in *Y*. These include potential low-frequency natural trends in ENSO itself and any delayed or non-linear impacts of ENSO on GMST and CREs. Consequently, this method likely yields a conservative estimate of the ENSO contribution (see Section 2.4) (Kelly and Jones, 1996; Compo and Sardeshmukh, 2010). Additional sensitivity analyses testing the assumptions of zero lag, linear trends, and ENSO linearity, via optimal lags, low-pass filtered GMST, and separate phase regressions, respectively, further confirm the robustness of the simplified model (see further details in Text S1 and Fig. S1).

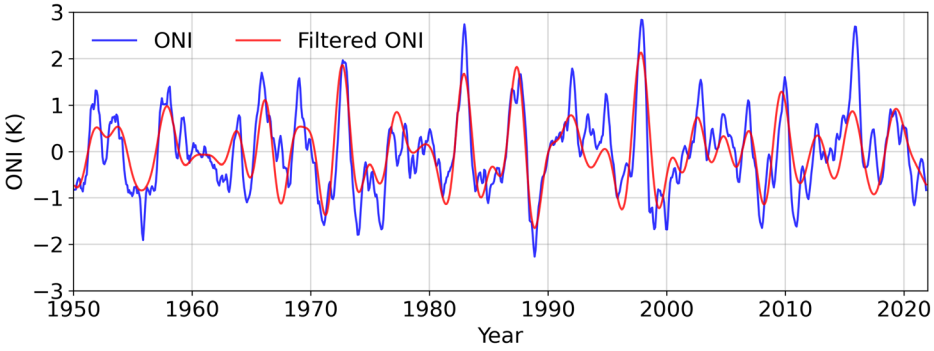

Figure 1: Time series of the original ONI (blue curve) and the bandpass-filtered ONI (red curve), derived from ERA5 data (January 1950–December 2021).

2.4 The estimation of ENSO contribution

To estimate the cloud feedback on global warming, following previous studies (e.g., Clement et al., 2009; Zhou et al., 2015; Uribe et al., 2022; Ceppi and Nowack, 2021; Dessler, 2010), we derive cloud feedback estimates by calculating the OLS regression slope between CRE and GMST (e.g., $\frac{\partial CRE_{net}}{\partial GMST}$). Although this slope technically differs from the true cloud feedback due to effects such as cloud masking, it serves as a valid proxy for our analysis. However, it is important to note that such a method inherently captures the influence of factors affecting both global temperature and cloud properties, such as ENSO, thereby confounding the true feedback with internal variability. To assess the corresponding ENSO contribution, we compute the difference between the results obtained before and after applying the ENSO-correction method. This difference, as formulated in Eq. (3):

$$ENSO_{con.} = \frac{\partial CRE}{\partial GMST} - \frac{\partial CRE_{corrected}}{\partial GMST_{corrected}} \quad (3),$$

is then used as a proxy measure of the ENSO contribution to cloud feedback estimates under global warming.

3 Results

3.1 ENSO's impact on the global-mean surface temperature

Figure 2 illustrates the impact of ENSO on GMST based on ERA5 data from January 1950 to December 2021.

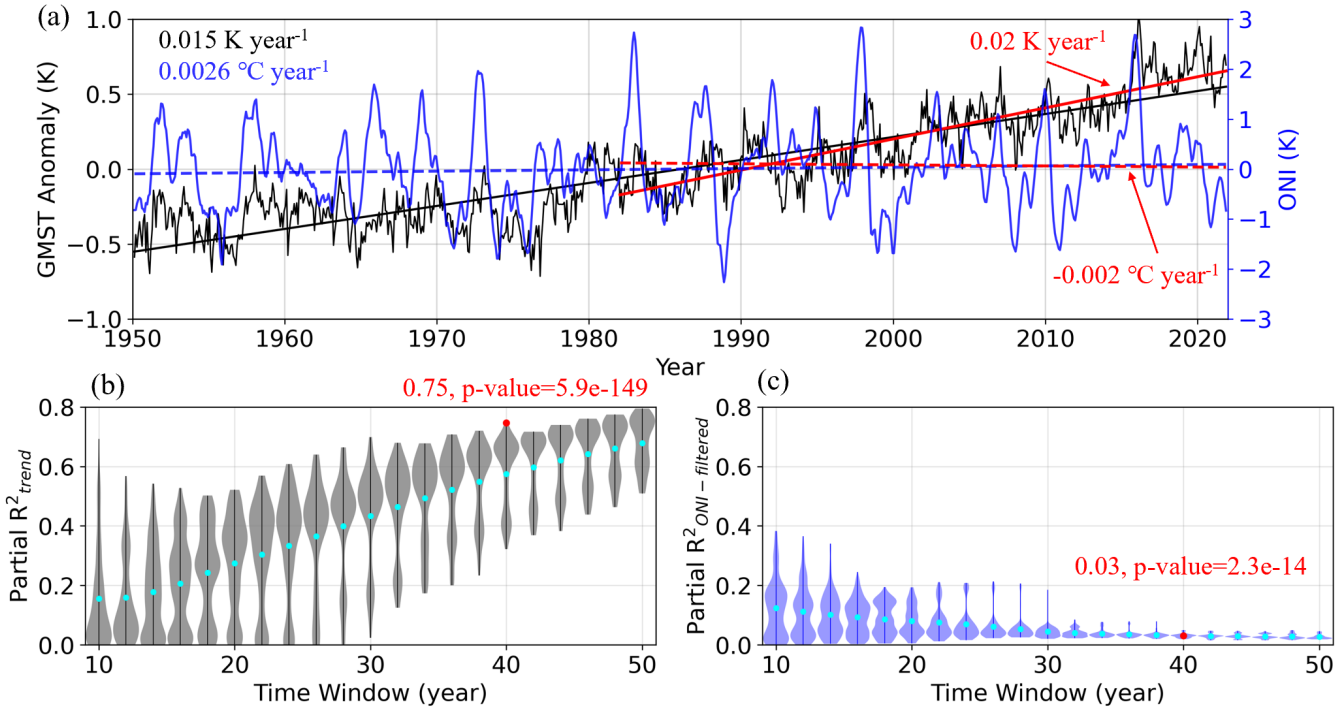

Figure 2: Analysis of the GMST variations driven by the temporal trend and ENSO, derived from ERA5 data (January 1950–December 2021). (a) Time series of GMST anomaly (black curve; left y-axis) and ONI (blue curve; right y-axis). The black and blue lines represent the corresponding OLS regression fits, with the values indicating their slopes. (b–c) Violin plots of (b) partial R^2_{trend} and (c) partial $R^2_{ONI\text{-}filtered}$ for GMST, shown as a function of the time window (2-year intervals). For each time window, the vertical line indicates the range (minimum to maximum), the shaded area represents the probability density, and the cyan dot denotes the mean value. The red lines, dots and numbers highlight the results for the selected representative 40-year subset (January 1982–December 2021) that is analyzed in Figs. 3–4. In panel (a), solid and dashed lines represent the statistically significant and insignificant trends at the 95% confidence level, respectively.

Figure 2a presents the time series of GMST anomalies (black curve) and the original ONI (blue curve). The corresponding OLS regression analysis reveals a consistent increase in GMST of 0.015 K year^{-1} (black line), which translates to an approximate 1 K of warming over the study period. This warming has been primarily attributed to rising CO_2 levels resulting from human activities (Eyring et al., 2021). In contrast, the ONI does not exhibit a statistically significant trend (blue dashed line), indicating no consistent long-term intensification or weakening of ENSO over recent decades. This finding aligns with results from 2 out of the 11 GCMs (GISS-E2-2-H and E3SM-1-0), which also show no significant ENSO trend in their historical simulations from 1950 to 2014 (not shown), indicating a widespread deficiency of current models in representing this historical feature of ENSO. Despite the lack of a long-term trend in ENSO, there is a clear covariation between GMST and ONI on interannual timescales, highlighting ENSO's significant impact on GMST. For example, the GMST difference

between the La Niña year of 1989 and the El Niño year of 1998 is approximately 0.8 K, a magnitude which is similar to the total linear warming over the entire 72-year period.

The relative contributions of the warming trend and ENSO to the variance of GMST depend on the analyzed timescale. To quantify this, we calculate the coefficient of partial determination (partial R^2) using OLS multivariate regression models (Eq. 1) and present the results as a function of the time window (ranging from 10 to 50 years, the upper limit of 50 years was selected to ensure an adequate sample size for robust analysis). The corresponding test statistics (Fig. S2) suggest that the ONI regression coefficient (*b* in Eq. 1) is statistically significant at the 95% confidence level across nearly all analyses, even when the explained variance is moderate. This allows us to assess the relative contribution of the warming trend (partial R^2_{trend}; Fig. 2b) and ENSO (partial $R^2_{ONI\text{-}filtered}$; Fig. 2c) to the total variance of GMST across different timescales with high confidence. The partial R^2_{trend} values increase consistently with longer time windows, suggesting that the warming trend accounts for a steadily growing proportion of GMST variance over extended periods. In contrast, the partial $R^2_{ONI\text{-}filtered}$ values decrease yet gradually stabilize for periods exceeding ~40 years, indicating a diminishing influence of ENSO as the timescale lengthens, though the rate of decline attenuates. This inverse relationship implies that the ENSO contribution to cloud feedback estimates becomes less substantial in longer periods. For instance, in the 40-year subset from January 1982–December 2021 (red dots in Figs. 2b–c), the warming trend explains approximately 75% of GMST variance, whereas ENSO accounts for only about 3%. The co-occurrence of this strong warming trend and the relatively weak ENSO signature, along with the stabilization of $R^2_{ONI\text{-}filtered}$ beyond 40 years, makes this period particularly informative for examining the ENSO contribution to cloud feedback estimates. It is therefore selected as a representative example to illustrate the methodology and resulting spatial patterns in Figs. 3–4. In addition, to account for the potential limitations of ONI in fully representing ENSO (Johnson, 2013), we conducted a similar analysis using six other ENSO indices and obtained similar results (see further details in Text S2 and Fig. S3).

3.2 ENSO's impact on cloud radiative effects

Results in Fig. 2 highlight the distinct time scales between the interannual variability of ENSO and the persistent long-term warming trend over recent decades. Historically, this difference has led to the neglect of the ENSO contribution when estimating cloud feedback over long periods. However, such neglect does not take into account the stronger impact of ENSO on cloud properties compared to that of recent warming (Li et al., 2021; Liu et al., 2023). To illustrate this point, we examine the same 40-year period (January 1982–December 2021) as an representative case and present the corresponding partial R^2 maps of CREs in Fig. 3. The maps of the corresponding residual R^2 are shown in Fig. S4.

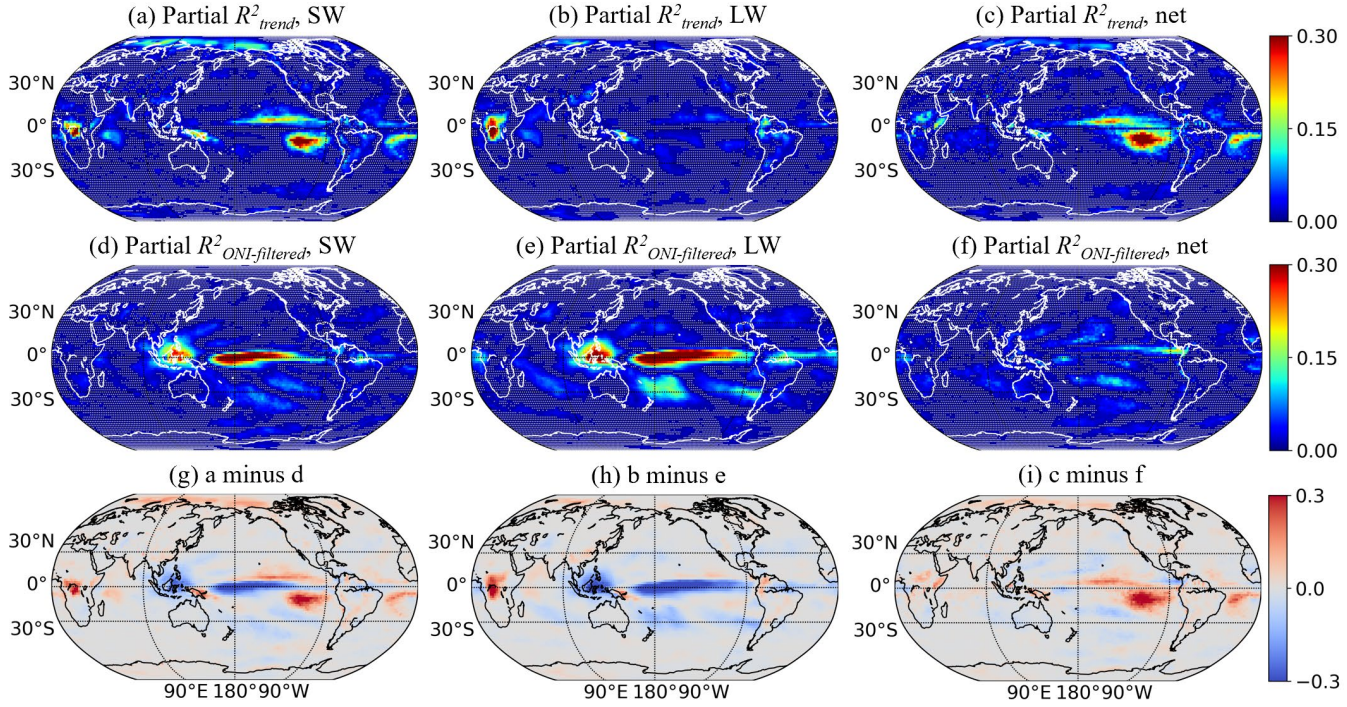

Figure 3: Analysis of variations in CREs driven by the temporal trend and ENSO, derived from ERA5 data (January 1982–December 2021). (a–c) Partial R^2_{trend} for (a) CRE_{SW}, (b) CRE_{LW}, and (c) CRE_{net}. (d–f) Partial $R^2_{ONI\text{-}filtered}$ for (d) CRE_{SW}, (e) CRE_{LW}, and (f) CRE_{net}. (g–i) The difference between (a–c) and (d–f). In panels (a–f), white dots denote grids with statistically insignificant partial regression coefficients for the corresponding variables (time for a–c; ONI for d–f) at the 95% confidence level.

Figures 3a–c show the spatial distribution of variations in CRE_{SW}, CRE_{LW}, and CRE_{net} attributed to the temporal trend (partial R^2_{trend}). High values indicate regions with a significant forced CRE signal. Given the significant warming trend in GMST during this period (0.02 K year^{-1}), the resulting patterns reveal strong co-variations between CREs and recent warming in regions such as the Arctic, central Africa, and the tropical eastern oceans. Figures 3d–f illustrate the variations in CREs attributed to ENSO (partial $R^2_{ONI\text{-}filtered}$). High values indicate regions where the CRE is dominated by ENSO-induced variability. These dominant spatial patterns align well with previous findings revealing the influence of ENSO on cloud properties (Yang et al., 2016; Li et al., 2021; Liu et al., 2023). Figures 3g–i display the difference between the two components (partial R^2_{trend} minus partial $R^2_{ONI\text{-}filtered}$). Compared to ENSO, the temporal trend has a much weaker impact on CREs over a large portion of the low- to mid-latitude oceans (blue shading in Figs. 3g–i). This is particularly evident for CRE_{SW} and CRE_{LW} across the Pacific, implying a region-dependent ENSO contribution to long-term cloud feedback estimates. Notably, outside the Pacific, CRE variations are generally weakly influenced by either of these factors, suggesting a potential role of other drivers or background noise.

3.3 ENSO contribution to historical cloud feedback estimates

Next, we examine the ENSO contribution (see Section 2.4) to historical cloud feedback estimates. To illustrate the methodology, Fig. 4 shows results for the same 40-year period (January 1982–December 2021) as an example. Prior to discussing the ERA5 results in detail, we conducted a similar analysis of ENSO contribution using the CERES data (for the period January 2002–December 2021) and compared the results of the two datasets (Fig. S5). The remarkably consistent patterns between ERA5- and CERES-based ENSO contributions indicate that ERA5 captures the essential features of ENSO-induced variations in CREs.

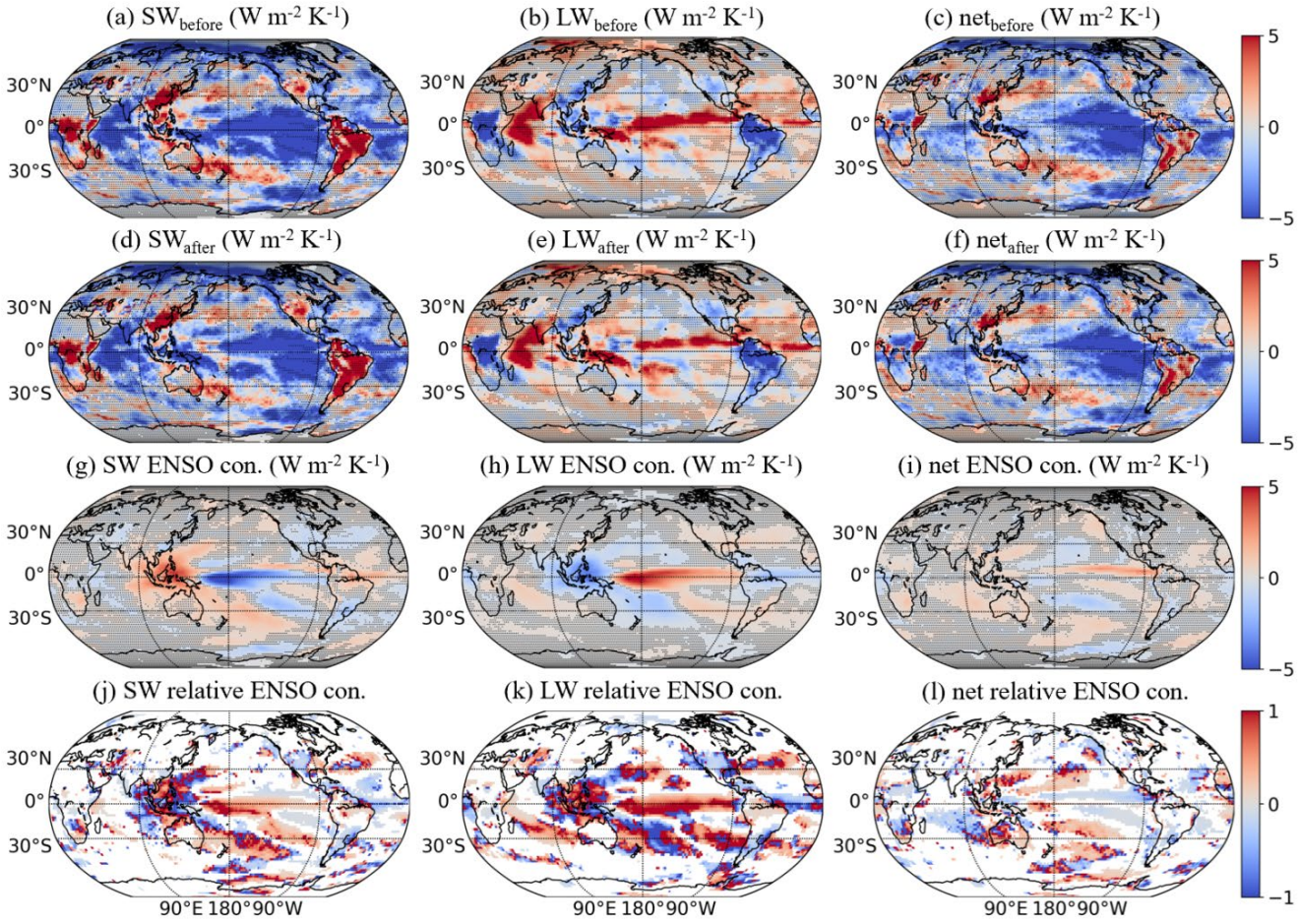

Figure 4: Analysis of the ENSO contribution to cloud feedback estimates for CRE$_{SW}$ (left column), CRE$_{LW}$ (middle column), and CRE$_{net}$ (right column), derived from ERA5 data (January 1982–December 2021). (a–c) Cloud feedback estimates before ENSO correction. (d–f) Cloud feedback estimates after ENSO correction. (g–i) ENSO contribution (a–c minus d–f). (j–l) Relative ENSO contribution (g–i divided by a–c). In panels (a–i), black dots denote grids with statistically insignificant partial regression coefficient of ONI (i.e., *b* in Eq. 1) for either GMST or respective CRE at the 95% confidence level. In panels (j–l), these insignificant grids are masked in white.

The ENSO contribution shown in Figs. 4g–i can be explained by the combined effects of ONI-explained variations in GMST (3%) and CREs, as discussed in Figs. 2–3. Again, as expected, the resulting patterns align closely with previous studies that documented ENSO's influence on cloud properties (Yang et al., 2016; Li et al., 2021; Liu et al., 2023) and the associated physical mechanisms (Taschetto et al., 2020). During the warm phase of ENSO (e.g., El Niño events), the anomalous warming of surface waters in the central to eastern tropical Pacific weakens the Walker circulation, suppressing updrafts over the western Pacific while enhancing convection over the central to eastern Pacific. These dynamical changes affect cloud formation and development, resulting in more and deeper (less and shallower) clouds over regions such as the central (western) tropical Pacific. Consequently, ENSO-driven changes in cloud properties lead to a negative (positive) contribution to shortwave cloud feedback estimates over the corresponding regions (Fig. 4g) and almost opposite changes for longwave (Fig. 4h), together leading to relatively weak and less distinct influence in the net cloud feedback estimates (Fig. 4i). Such physical consistency further validates the reliability of our regression-based ENSO-correction method.

Figures 4j–l show the distributions of the relative ENSO contribution, which is calculated as the ratio of the ENSO contribution (Figs. 4g–i) to the original cloud feedback estimates (Figs. 4a–c). The ratio reaches ±1 (dark reddish and bluish shades) over a substantial part of low- to mid-latitude oceans, indicating comparable ENSO- and non-ENSO-forced cloud feedback over these regions. But, by definition, the robustness of this relative metric is susceptible to near zero denominators and should be interpreted with caution.

As shown in Fig. 2, the impact of ENSO on GMST varies depending on the period under examination. To quantify this timescale dependence, we calculate the ENSO contribution (e.g., Figs. 4g–i) for the same range of possible periods by applying each time window across the entire 72 years and introduce a metric we call "ENSO effect minimal time". This metric is defined as the shortest time window beyond which the mean magnitude of ENSO contribution (ignoring the sign) falls and remains below 1 W m^{-2} K^{-1} (i.e., $|\overline{ENSO\ con.}| < 1\ W\ m^{-2}\ K^{-1}$), or beyond which the partial regression coefficient of ONI (i.e., b in Eq. 1) for either GMST or CRE becomes and remains statistically insignificant at the 95% confidence level. The threshold of 1 W m^{-2} K^{-1} is chosen to signify a non-negligible ENSO contribution relative to the local cloud feedback estimates, which is typically on the order of several W m^{-2} K^{-1}, as simulated by current GCMs (Forster et al., 2021; Ceppi & Nowack, 2021; Zelinka et al., 2016; Myers et al., 2021).

Figure 5 presents the spatial distribution of "ENSO effect minimal time" for CRE_{SW}, CRE_{LW}, and CRE_{net}, revealing complex patterns and notable differences among the three variables. In most subtropical regions, the minimal time is less than 30 years (bluish to greenish shades). However, in some tropical and mid-latitude regions, particularly the Pacific Ocean, the mean ENSO contribution never consistently falls below 1 W m^{-2} K^{-1} or becomes statistically insignificant within time windows up to 50 years (white shades). These results align with the slow decay of ENSO impact on GMST (Fig. 2c) and the patterns revealed for ENSO impact on CREs (Figs. 3d–f), illustrating clearly that ENSO contributes significantly to the the estimation of long-term cloud feedback, especially over the Pacific and during relatively short periods characterized by intense ENSO activity.

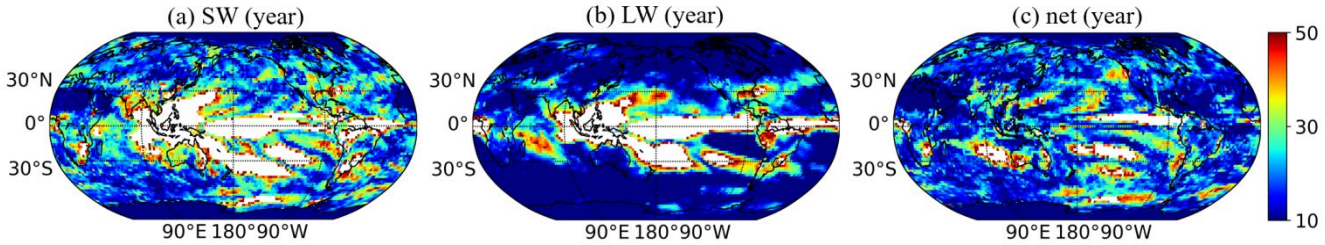

Figure 5: Spatial distribution of the "ENSO effect minimal time" for different CREs derived from ERA5 data (January 1982–December 2021). (a) CRE_{SW}, (b) CRE_{LW}, and (c) CRE_{net}. Regions masked in white denote grids where the ENSO contribution never consistently falls below 1 W m^{-2} K^{-1} or becomes statistically insignificant within time windows up to 50 years.

Figure 6 presents the ENSO contribution to global-mean CREs as a function of the time window. The corresponding results derived from CERES measurements, ERA5 data during the CERES period, and ERA5 data during the representative 40-year subset are also shown. As expected, the results change with time and converge toward small values (about 0.1, 0.0, and 0.1 W m^{-2} K^{-1} for CRE_{SW}, CRE_{LW}, and CRE_{net}, respectively) due to the cancellation of positive and negative local ENSO contributions across different regions. This convergence also agrees well with the behavior of ENSO impact on GMST in Fig. 2c.

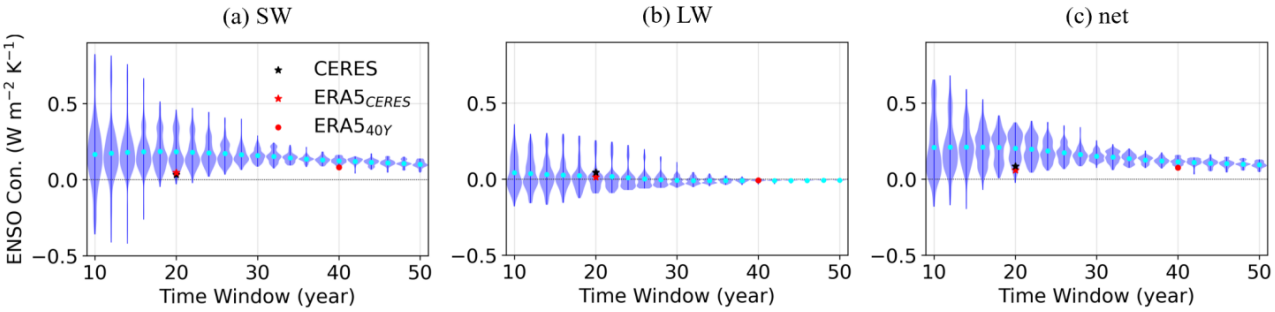

Figure 6: Violin plots of the ENSO contribution to global-mean CREs derived from ERA5 data (January 1950–December 2021). (a) CRE_{SW}, (b) CRE_{LW}, and (c) CRE_{net}. The black star, red star, and red dot denote the results from CERES measurements, ERA5 data during the CERES period, and ERA5 data during the representative 40-year period, respectively.

To provide a partial validation of our findings using current climate models, taking the CRE_{net} as an example, we analyzed the "ENSO effect minimal time" and the global-mean ENSO contribution for 11 GCM simulations of the historical experiment (Figs. S6–S7). While substantial inter-model discrepancies exist, the fundamental finding that ENSO can significantly affect long-term cloud feedback estimates remains robust. The discrepancies between the models indicate deficiencies in the ability of models to accurately represent ENSO, global warming, and their relative impacts on GMST and cloud properties (Bellenger et al., 2014; Coburn and Pryor, 2021).

3.4 ENSO contribution to cloud feedback projections

To link our findings to climate projections, we analyze the first 150 years of 11 GCM simulations from the abrupt-4×CO_2 experiment. Figure 7 presents the spatial distribution of the ENSO contribution to CRE_{net}, with the corresponding relative contribution shown in Fig. 8.

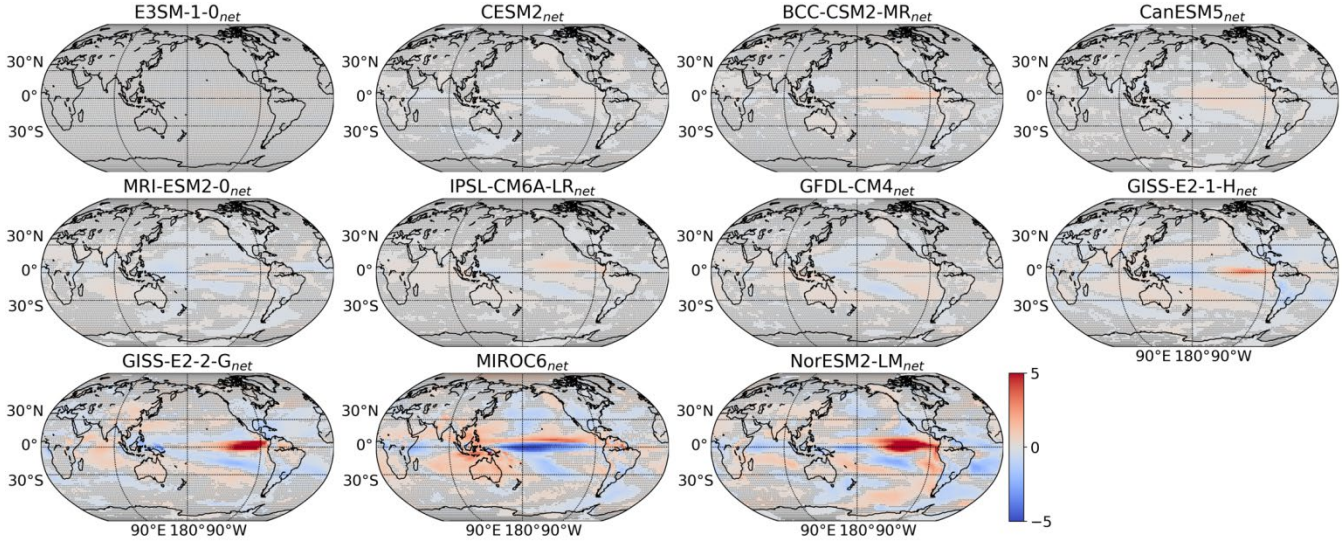

Figure 7: Maps of ENSO contribution to CRE_{net} derived from GCM simulations of the abrupt-4×CO_2 experiment (first 150 years). The corresponding model name is indicated in each panel. Black dots denote grids with statistically insignificant partial regression coefficient of ONI (i.e., *b* in Eq. 1) for either GMST or CRE at the 95% confidence level.

Again, significant ENSO contributions are evident worldwide, especially over the Pacific Ocean. However, substantial discrepancies in terms of both patterns and magnitudes exist among GCMs. More specifically, Fig. 7 shows a predominantly positive ENSO contribution (reddish shades) over the eastern tropical Pacific and a predominantly negative ENSO contribution (bluish shades) over the western tropical Pacific, indicating that the analyzed GCMs capture the broad structure of cloud response to ENSO to some extent. However, the specific magnitudes and detailed spatial features vary considerably across the 11 models. For instance, simulations from GISS-E2-2-G, MIROC6, and NorESM2-LM show that the ENSO contribution to cloud feedback estimates remains on the order of a few W m^{-2} K^{-1} over extensive regions, even for a 150-year period, which is comparable to the local cloud feedback estimates (Forster et al., 2021; Ceppi & Nowack, 2021; Zelinka et al., 2016; Myers et al., 2021). Further analysis (Fig. S8) reveals that the substantial ENSO contributions found in these models are primarily driven by their strong ENSO variability (Fig. S8a), while the ENSO sensitivity (b in Eq. 1) plays a secondary role (Fig. S8b). Notably, these models also tend to exhibit stronger forced cloud feedback estimates (Fig. S8c). Such relationships align with and extend previous studies that identified robust correlations between interannual and long-term cloud feedback (e.g., Zhou et al., 2015; Dessler and Forster, 2018; Davis et al., 2024) by highlighting the potential modulating role of ENSO contributions.

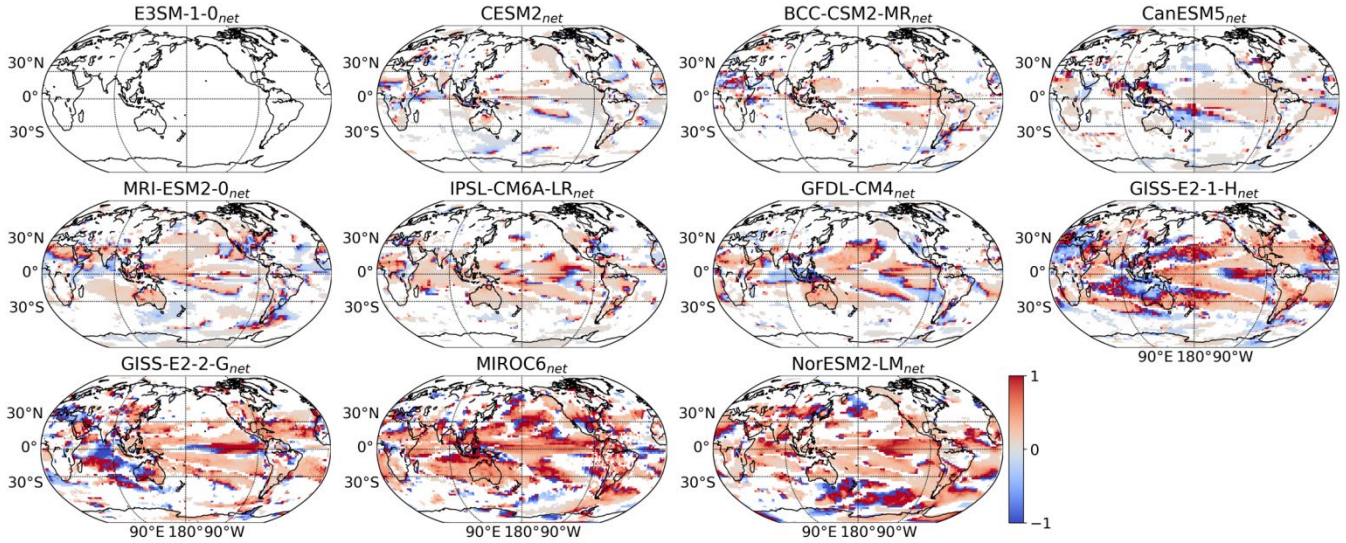

Figure 8: Maps of the relative ENSO contribution to CRE_{net} derived from GCM simulations of the abrupt-4×CO_2 experiment (first 150 years). The corresponding model name is indicated in each panel. Grids with statistically insignificant partial regression coefficient of ONI (i.e., *b* in Eq. 1) for either GMST or CRE at the 95% confidence level are masked in white.

The ENSO contribution to global-mean CRE_{net} (Fig. 9) also exhibits large inter-model spread as well. As discussed above, these differences indicate deficiencies of models in accurately representing ENSO, global warming, and their relative impacts on GMST and clouds (Bellenger et al., 2014; Coburn and Pryor, 2021). For example, previous studies suggest that, compared to observations, many GCMs present exhibit an overly strong equatorial Pacific cold tongue (Jiang et al., 2021) and fail to capture the recent strengthening of the zonal equatorial Pacific SST gradient (Seager et al., 2019). These two deficiencies introduce critical uncertainties into projections of ENSO, and hence clouds, under global warming (e.g., Guilyardi et al., 2020; Beobide-Arsuaga et al., 2021). The time series of GMST and global-mean CREnet for two representative GCMs (E3SM-1-0 and NorESM2-LM) are also shown in Fig. S9. The results demonstrate a clear separation between the trend- and ONI-related variations achieved by our regression-based ENSO-correction method, thereby providing further validation for the ENSO contribution derived using this method.

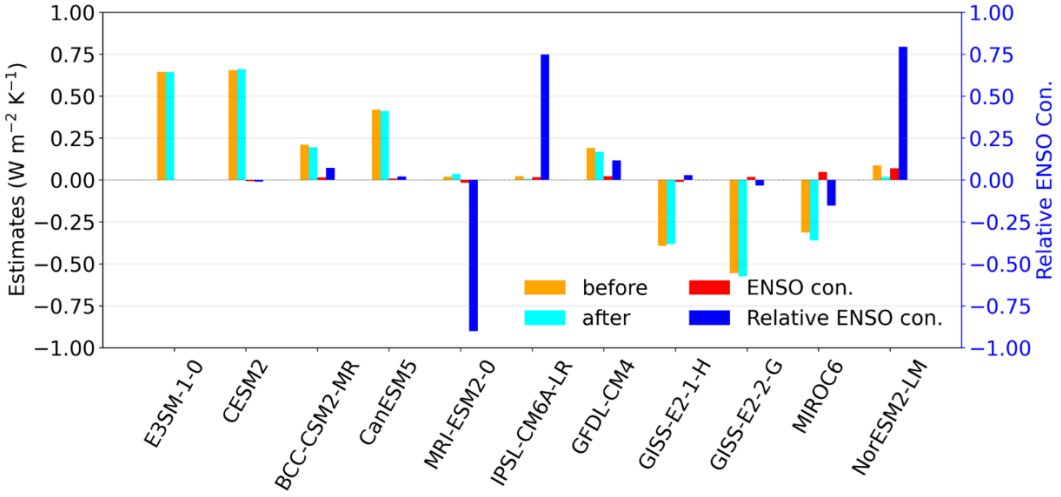

Figure 9: Bar charts of the ENSO contribution to global-mean CRE_{net} derived from GCM simulations of the abrupt-4×CO_2 experiment (first 150 years). The orange and cyan bars indicate global-mean cloud feedback estimates before and after the ENSO correction, respectively. The red bars indicate the ENSO contribution (orange minus cyan). The blue bars indicate relative ENSO contribution (red divided by orange; right y-axis). Note that a large relative value (blue bar) can arise when the original feedback estimate (orange bar) is small.

4 Discussion

ENSO is a natural interannual climate phenomenon characterized by anomalous sea-surface temperature and pressure in the tropical Pacific Ocean. It influences global temperature and cloud properties (Davey et al., 2014; Cai et al., 2019; Taschetto et al., 2020), thereby affecting the accuracy of cloud feedback estimates under global warming (Zhou et al., 2015; Uribe et al., 2022; Richardson et al., 2022; Jin et al., 2024). This study quantifies such ENSO contribution using 72 years of ERA5 data and 150 years of simulations from 11 GCMs. The results reveal that regression-based cloud feedback estimates are susceptible to a significant ENSO impact, even on decadal and centennial timescales. A regression-based ENSO-correction method was then applied to correct for ENSO's influence and quantify its contribution. The findings show that the magnitude of this contribution exhibits strong regional and temporal dependence. In most subtropical regions, the ENSO contribution likely falls below 1 W m^{-2} K^{-1} for periods longer than 30 years. However, in many tropical regions, the contribution remains statistically significant and can exceed 1 W m^{-2} K^{-1}, even for periods longer than 50 years (the maximum time window analyzed). These results highlight the importance of incorporating an ENSO-correction procedure when assessing the forced cloud feedback, particularly in tropical regions and for short periods characterized by intense ENSO activity.

The study acknowledges several limitations, including its inability to account for non-linear or delayed ENSO effects (Compo and Sardeshmukh, 2010) and the sensitivity of the "ENSO effect minimal time" to the chosen threshold and dataset used. As a result, the findings should be regarded as conservative estimates and the quantitative conclusions should be interpreted with caution, particularly in the context of GCM simulations. Notwithstanding these limitations, the study provides a straightforward method to approximate the ENSO contribution, offering valuable insights into the influence of ENSO on

cloud feedback estimates. The implications of this research are twofold. First, it quantitatively assesses the spatial distribution and timescales of the ENSO contribution to regression-based cloud feedback estimates. Second, given the known deficiencies in GCMs' representation of ENSO and its dynamics (Bellenger et al., 2014; Coburn and Pryor, 2021; Jiang et al., 2021; Seager et al., 2019), coupled with substantial uncertainties in future ENSO projections (Guilyardi et al., 2020; Beobide-Arsuaga et al., 2021), the revealed significant impact of ENSO on warming and cloud properties poses a critical challenge to the reliability of climate projections.

Code and data availability. All analyses used to generate results are conducted by the standard functions/algorithms offered by the programming languages of Python (Version 3.7.0, https://www.python.org/). The SciPy library (Version 1.5.2) for Pearson *r* and OLS regression is publicly available at https://scipy.org/. The pyMannKendall library (Version 1.4.3) for Hamed and Rao modified Mann-Kendall trend test is publicly available at https://pypi.org/project/pymannkendall/. All data used in this work is publicly available. ERA5 data was downloaded from the Copernicus Climate Change Service Climate Data Store (https://doi.org/10.24381/cds.f17050d7; accessed on 12 March 2023). ENSO indexes used in the Supplementary Information (TNI, SOI, and BEST) were downloaded from the NOAA center (https://psl.noaa.gov/enso/dashboard.html; accessed on 20 May 2023). GCM simulations were downloaded from the Earth System Grid Federation (https://esgf-node.llnl.gov/search/cmip6/; accessed on 6 December 2024).

Author contributions. H.L.: Formal analysis, Conceptualization, Methodology, Writing–Original Draft. I.K.: Conceptualization, Methodology, Supervision. O.A.: Conceptualization, Methodology, Writing–Review & Editing. S.M.: Formal analysis. All authors discussed the results, contributed to the final manuscript, and approved the submitted version.

Competing interests. The authors declare they have no conflict of interest.

Financial support. This work has been supported by the National Natural Science Foundation of China (No. 42405088), the European Research Council (ERC) under the European Union's Horizon 2020 research and innovation program (grant agreement No. 810370), and the Independent Research Project of the Innovation Talent Program (No. 202401-YJRC-XX-033).

References

Angell, J. K.: Tropospheric temperature variations adjusted for El Niño, 1958–1998, J. Geophys. Res. Atmos., 105, 11841–11849, doi:10.1029/2000JD900044, 2000.

Bellenger, H., Guilyardi, E., Leloup, J., Lengaigne, M. and Vialard, J.: ENSO representation in climate models: From CMIP3 to CMIP5, Clim. Dyn., 42, 1999–2018, doi:10.1007/s00382-013-1783-z, 2014.

Beobide-Arsuaga, G., Bayr, T., Reintges, A. and Latif, M.: Uncertainty of ENSO-amplitude projections in CMIP5 and CMIP6 models, Clim. Dyn., 56, 3875–3888, doi:10.1007/s00382-021-05673-4, 2021.

Binder, H., Boettcher, M., Joos, H., Sprenger, M. and Wernli, H.: Vertical cloud structure of warm conveyor belts–a comparison and evaluation of ERA5 reanalysis, CloudSat and CALIPSO data, Weather Clim. Dyn., 1, 577–595, doi:10.5194/wcd-1-577-2020, 2020.

Cai, W. et al.: Pantropical climate interactions, Science, 363, eaav4236, doi:10.1126/science.aav423, 2019.

Ceppi, P. and Nowack, P.: Observational evidence that cloud feedback amplifies global warming, Proc. Natl. Acad. Sci., 118, e2026290118, doi:10.1073/pnas.2026290118, 2021.

Chen, T., Rossow, W.B., and Zhang, Y.: Radiative effects of cloud-type variations, J. Clim., 13, 264–286, doi:10.1175/1520-0442(2000)013<0264:REOCTV>2.0.CO;2, 2000.

Clement, A. C., Burgman, R. and Norris, J. R.: Observational and Model Evidence for Positive Low-Level Cloud Feedback, Science, 325, 460–464, doi:10.1126/science.11712, 2009.

Coburn, J. and Pryor, S. C.: Differential Credibility of Climate Modes in CMIP6, J. Clim., 34, 8145–8164, doi:10.1175/JCLI-D-21-0359.1, 2021.

Compo, G. P. and Sardeshmukh, P. D.: Removing ENSO-related variations from the climate record, J. Clim., 23, 1957–1978, doi:10.1175/2009JCLI2735.1, 2010.

Davey, M., Brookshaw, A. and Ineson, S.: The probability of the impact of ENSO on precipitation and near-surface temperature, Clim. Risk Manag., 1, 5–24, doi:10.1016/j.crm.2013.12.002, 2014.

Davis, L. L. B., Thompson, D. W. J., Rugenstein, M. and Birner, T.: Links between internal variability and forced climate feedbacks: The importance of patterns of temperature variability and change. Geophys. Res. Lett., 51, e2024GL112774, doi.org/10.1029/2024GL112774, 2024.

Dessler, A. E.: A determination of the cloud feedback from climate variations over the past decade, Science, 330, 1523–1527, doi:10.1126/science.1192546, 2010.

Dessler, A. E. and Forster, P. M.: An estimate of equilibrium climate sensitivity from interannual variability. J. Geophys. Res. Atmos., 123, 8634-8645, https://doi.org/10.1029/2018JD028481, 2018.

Eleftheratos, K., Zerefos, C., Varotsos, C. and Kapsomenakis, I.: Interannual variability of cirrus clouds in the tropics in el niño southern oscillation (ENSO) regions based on international satellite cloud climatology project (ISCCP) satellite data, Int. J. Remote Sens., 32, 6395–6405, doi:10.1080/01431161.2010.510491, 2011.

Eyring, V., Bony, S., Meehl, G. A., Senior, C. A., Stevens, B., Stouffer, R. J., and Taylor, K. E.: Overview of the Coupled Model Intercomparison Project Phase 6 (CMIP6) experimental design and organization, Geosci. Model Dev., 9, 1937–1958, doi:10.5194/gmd-9-1937-2016, 2016.

Eyring, V., Gillett, N. P., Achuta Rao, K. M., Barimalala, R., Barreiro Parrillo, M., Bellouin, N. et al.: Human Influence on the Climate System, in Climate Change 2021: The Physical Science Basis, Contribution of Working Group I to the Sixth Assessment Report of the Intergovernmental Panel on Climate Change (Cambridge University), doi:10.1017/9781009157896.005, 2021.

Forster, P., Storelvmo, T., Armour, K., Collins, W., Dufresne, J. L., Frame, D. et al.: The Earth's Energy Budget, Climate Feedbacks, and Climate Sensitivity, in Climate Change 2021: The Physical Science Basis, Contribution of Working Group I to the Sixth Assessment Report of the Intergovernmental Panel on Climate Change (Cambridge University), doi:10.1017/9781009157896.009, 2021.

Glantz, M. H. and Ramirez, I. J.: Reviewing the oceanic Nino index (ONI) to enhance societal readiness for El Niño's impacts, Int. J. Disaster Risk Sci., 11, 394–403, doi:10.1007/s13753-020-00275-w, 2020.

Guan, B. and Nigam, S.: Pacific Sea Surface Temperatures in the Twentieth Century: An Evolution-Centric Analysis of Variability and Trend, J. Clim., 21, 2790–2809, doi:10.1175/2007JCLI2076.1, 2008.

Guilyardi, E., Capotondi, A., Lengaigne, M., Thual, S. and Wittenberg, A. T.: ENSO Modeling: History, Progress, and Challenges, in El Niño Southern Oscillation in a Changing Climate (American Geophysical Union), doi:10.1002/9781119548164.ch9, 2020.

Gulev, S. K., Thorne, P. W., Ahn, J., Dentener, F. J., Domingues, C. M., Gong, D. et al.: Changing State of the Climate System, in Climate Change 2021: The Physical Science Basis, Contribution of Working Group I to the Sixth Assessment Report of the Intergovernmental Panel on Climate Change (Cambridge University), doi:10.1017/9781009157896.004, 2021.

Hamed, K. H. and Rao, A. R.: A modified Mann-Kendall trend test for autocorrelated data, J. Hydrol., 204, 182-196, doi:10.1016/S0022-1694(97)00125-X, 1998.

Hersbach, H., Bell, B., Berrisford, P., Hirahara, S., Horányi, A., Muñoz-Sabater, J. et al.: The ERA5 global reanalysis, Q. J. R. Meteorol. Soc., 146, 1999–2049, doi:10.1002/qj.3803, 2020.

Hersbach, H. Bell, B., Berrisford, P., Biavati, G., Horányi, A., Muñoz-Sabater, J. et al.: ERA5 monthly averaged data on single levels from 1940 to present [Dataset], Copernicus Climate Change Service (C3S) Climate Data Store (CDS), doi:10.24381/cds.f17050d7, 2023.

Hope, P., Henley, B. J., Gergis, J., Brown, J. and Ye, H.: Time-varying spectral characteristics of ENSO over the Last Millennium, Clim. Dyn., 49, 1705–1727, doi:10.1007/s00382-016-3393-z, 2017.

Hussain, M. M. and Mahmud, I.: pyMannKendall: a python package for non parametric Mann Kendall family of trend tests [Software], J. Open Source Softw., 4, 1556, doi:10.21105/joss.01556, 2019.

Jiang, W., Huang, P., Huang, G. and Ying, J.: Origins of the Excessive Westward Extension of ENSO SST Simulated in CMIP5 and CMIP6 Models, J. Clim., 34, 2839–2851, doi:10.1175/JCLI-D-20-0551.1, 2021.

Jin, D., Kramer R. J., Oreopoulos, L. and Lee D.: ENSO disrupts boreal winter CRE feedback, J. Clim., 37, 585–603, doi:10.1175/JCLI-D-23-0282.1, 2024.

Johnson, N. C.: How many ENSO flavors can we distinguish?, J. Clim., 26, 4816–4827, doi:10.1175/JCLI-D-12-00649.1, 2013.

Kelly, P. M. and Jones, P. D.: Removal of the El Niño-Southern Oscillation signal from the gridded surface air temperature data set, J. Geophys. Res. Atmos., 101, 19013–19022, doi:10.1029/96JD01173, 1996.

Li, Y. et al.: Pairwise-rotated EOFs of global cloud cover and their linkages to sea surface temperature, Int. J. Climatol., 41, 2342–2359, doi:10.1002/joc.6962, 2021.

Liu, H., Koren, I., Altaratz, O. and Chekroun, M. D.: Opposing trends of cloud coverage over land and ocean under global warming, Atmos. Chem. Phys., 23, 6559–6569, doi:10.5194/acp-23-6559-2023, 2023.

Loeb, N. G., Doelling, D. R., Wang, H., Su, W., Nguyen, C., Corbett, J. G., et al.: Clouds and the earth's radiant energy system (CERES) energy balanced and filled (EBAF) top-ofatmosphere (TOA) edition-4.0 data product, J. Clim., 31, 895-918, doi.org/10.1175/JCLI-D-17-0208.1, 2018.

Madenach, N., Carbajal Henken, C., Preusker, R., Sourdeval, O. and Fischer, J.: Analysis and quantification of ENSO-linked changes in the tropical atlantic cloud vertical distribution using 14 years of MODIS observations, Atmos. Chem. Phys., 19, 13535–13546, doi:10.5194/acp-19-13535-2019, 2019.

Myers, T. A., Scott, R. C., Zelinka, M. D., Klein, S. A., Norris, J. R. and Caldwell, P. M.: Observational constraints on low cloud feedback reduce uncertainty of climate sensitivity, Nat. Clim. Chang., 11, 501–507, doi:10.1038/s41558-021-01039-0, 2021.

Neelin, J. D., Battisti, D. S., Hirst, A. C., Jin, F. F., Wakata, Y., Yamagata, T. et al.: ENSO theory, J. Geophys. Res.: Oceans, 103, 14261–14290, doi:10.1029/97JC03424, 1998.

Park, S. and Leovy C. B.: Marine low-cloud anomalies associated with ENSO, J. Clim., 17, 3448–3469, doi:10.1175/1520-0442(2004)017<3448:MLAAWE>2.0.CO;2, 2004.

Penland, C. and Matrosova, L.: Studies of El Niño and interdecadal variability in tropical sea surface temperatures using a nonnormal filter, J. Clim., 19, 5796–5815, doi:10.1175/JCLI3951.1, 2006.

Richardson, M. T., Roy, R. J. and Lebsock, M. D.: Satellites suggest rising tropical high cloud altitude: 2002–2021, Geophys. Res. Lett., 49, e2022GL098160, doi:10.1029/2022GL098160, 2022.

Seager, R., Cane, M., Henderson, N., Lee, D. E., Abernathey, R. and Zhang, H.: Strengthening tropical Pacific zonal sea surface temperature gradient consistent with rising greenhouse gases, Nat. Clim. Chang., 9, 517-522, doi:10.1038/s41558-019-0505-x, 2019.

Sherwood, S. C., Webb, M. J., Annan, J. D., Armour, K. C., Forster, P. M., Hargreaves, J. C. et al.: An assessment of Earth's climate sensitivity using multiple lines of evidence. Rev. Geophys., 58, e2019RG000678, doi.org/10.1029/2019RG000678, 2020.

Stephens, G. L., Li, J., Wild, M., Clayson C. A., Loeb, N., Kato, S. et al.: An update on Earth's energy balance in light of the latest global observations, Nat. Geosci., 5, 691–696, doi:10.1038/ngeo1580, 2012.

Stubenrauch, C. J., Rossow, W. B., Kinne S., Ackerman, S., Cesana G., Chepfer, H. et al.: Assessment of global cloud datasets from satellites: Project and database initiated by the GEWEX radiation panel, Bull. Amer. Meteor. Soc., 94, 1031–1049, doi:10.1175/BAMS-D-12-00117.1, 2013.

Taschetto, A. S., Ummenhofer, C. C., Stuecker, M. F., Dommenget, D., Ashok, K., Rodrigues, R. R. et al.: ENSO Atmospheric Teleconnections, in El Niño Southern Oscillation in a Changing Climate (American Geophysical Union), doi:10.1002/9781119548164.ch14, 2020.

Teng, H. F., Lee, C. S. and Hsu, H. H.: Influence of ENSO on formation of tropical cloud clusters and their development into tropical cyclones in the western north pacific, Geophys. Res. Lett., 41, 9120–9126, doi:10.1002/2014GL061823, 2014.

Uribe, A., Bender, F. A. M. and Mauritsen, T.: Observed and CMIP6 modeled internal variability feedbacks and their relation to forced climate feedbacks, Geophys. Res. Lett., 49, e2022GL100075, doi:10.1029/2022GL100075, 2022.

Virtanen, P., Gommers, R., Oliphant, T. E., Haberland M., Reddy, T., Cournapeau, D. et al.: SciPy 1.0: Fundamental Algorithms for Scientific Computing in Python, Nat. Methods, 17, 261-272, doi:10.1038/s41592-019-0686-2., 2020.

Webb, M. J., Andrews, T., Bodas-Salcedo, A., Bony, S., Bretherton, C. S., Chadwick, R. et al.: The Cloud Feedback Model Intercomparison Project (CFMIP) contribution to CMIP6, Geosci. Model Dev., 10, 359-384, doi:10.5194/gmd-10-359-2017, 2017.

Yang, Y., Russell, L. M., Xu, L., Lou, S., Lamjiri, M. A., Somerville, R. C. J. et al.: Impacts of ENSO events on cloud radiative effects in preindustrial conditions: changes in cloud fraction and their dependence on interactive aerosol emissions and concentrations, J. Geophys. Res. Atmos., 121, 6321–6335, doi:10.1002/2015JD024503, 2016.

Yao, B., Teng, S., Lai, R., Xu, X., Yin, Y., Shi, C. et al.: Can atmospheric reanalyses (CRA and ERA5) represent cloud spatiotemporal characteristics?. Atmos. Res., 244, 105091, doi:10.1016/j.atmosres.2020.105091, 2020.

Zelinka, M. D., Zhou, C. and Klein, S. A.: Insights from a refined decomposition of cloud feedbacks, Geophys. Res. Lett., 43, 9259–9269, doi:10.1002/2016GL069917, 2016.

Zelinka, M. D., Myers, T. A., McCoy, D. T., Po-Chedley, S., Caldwell, P. M., Ceppi, P. et al.: Causes of higher climate sensitivity in cmip6 models, Geophys. Res. Lett., 47, 2019–085782, doi:10.1029/2019GL085782, 2020.

Zhou, C., Zelinka, M. K., Dessler, A. E., and Klein S. A.: The relationship between interannual and long-term cloud feedbacks, Geophys. Res. Lett., 42, 10–463, doi:10.1002/2015GL066698, 2015.